Optical Control of Nanoparticle Catalysis Influenced by Photoswitch Positioning in Hybrid Peptide Capping Ligands

Randy L. Lawrence,[1] Zak E. Hughes,[2,†] Vincent J. Cendan,[1] Yang Liu,[3] Chang-Keun Lim,[4] Paras N. Prasad,[4] Mark T. Swihart,[3] Tiffany R. Walsh,[2] Marc R. Knecht[1,*]

1. Department of Chemistry, University of Miami, 1301 Memorial Drive, Coral Gables, Florida 33146, United States

2. Institute for Frontier Materials, Deakin University, Geelong, VIC 3216, Australia

3. Department of Chemical and Biological Engineering and 4. Department of Chemistry and Institute for Lasers, Photonics, and Biophotonics, University at Buffalo, The State University of New York, Buffalo, New York 14260, United States

KEYWORDS Au nanoparticles, peptides, biointerface reconfiguration, catalysis, photoactivated switch

ABSTRACT: Here we present an in-depth analysis of structural factors that modulate peptide-capped nanoparticle catalytic activity via optically driven structural reconfiguration of the biointerface present at the particle surface. Six different sets of peptide-capped Au nanoparticles were prepared, in which an azobenzene photoswitch was incorporated into one of two well-studied peptide sequences with known affinity for Au, each at one of three different positions: The N- or C-terminus, or mid-sequence. Changes in the photoswitch isomerization state induce a reversible structural change in the surface-bound peptide, which modulates the catalytic activity of the material. This control of reactivity is attributed to changes in the amount of accessible metallic surface area available to drive the reaction. This research specifically focuses on the effect of the peptide sequence and photoswitch position in the biomolecule, from which potential target systems for on/off reactivity have been identified. Additionally, trends associated with photoswitch position for a peptide sequence (Pd4) have been identified. Integrating the azobenzene at the N-terminus or central region results in nanocatalysts with greater reactivity in the *trans* and *cis* conformations, respectively; however, positioning the photoswitch at the C-terminus gives rise to a unique system that is reactive in the *trans* conformation and partially deactivated in the *cis* conformation. These results provide a fundamental basis for new directions in nanoparticle catalyst development to control activity in real time, which could have significant implications in the design of catalysts for multistep reactions using a single catalyst. Additionally, such a fine level of interfacial structural control could prove to be important for applications beyond catalysis, including biosensing, photonics, and energy technologies that are highly dependent on particle surface structures.

Introduction

Catalytic nanoparticles (NPs) provide new pathways for chemical transformation processes, advancing these approaches toward a sustainable future.[1-4] Typically, such materials are stabilized in colloidal suspension by organic ligands covalently bound to the particle surface.[5-6] While these ligands are required for stability, they can hamper reactivity by blocking reactant access to the catalytic surface.[7] Moreover, they are rigidly attached to the NPs in a single conformation, such that their influence on the catalytic process is fixed. By advancing the capabilities of the ligand layer, new functions could be integrated into the NP catalytic system, such as controllable on/off reactivity and substrate selectivity.

Recently, we have demonstrated that peptides with azobenzene photoswitches integrated into their biomolecular structure can provide a unique photoresponsive NP biointerface that allows for remote optical manipulation of the particle's catalytic properties.[8] In this approach, the modified AuBP1 peptide (WAGAKRLVLRRE), identified for its affinity for Au, non-covalently interacts with the noble metal surface, stabilizing the colloidal dispersion in water.[9-10] With the photoswitch in the *trans* configuration, the biomolecules adopt an initial conformation. Then, upon optical triggering, the azobenzene isomerizes to the *cis* conformation.[11] This isomerization event is propagated throughout the peptide, causing the entire biomolecular overlayer structure on the NP surface to adopt a different configuration.[12-13] Using light, these overlayer structures can be reversibly switched between the two conformations, thus presenting two substantially different NP surface structures in solution. In this manner, different catalytic capabilities can be achieved from the same Au NPs depending

upon the peptide surface configuration.[8] For instance, using the reduction of 4-nitrophenol to 4-aminophenol as a model reaction, the reactivity for Au NPs capped with the AuBP1 peptide with the photoswitch at the N-terminus demonstrated notably higher activity with the azobenzene molecule in the *trans* conformation compared to the *cis* conformation.

While peptide sequence plays a central role in determining biomolecular NP surface structure, the position of the photoswitch can also drive adoption of different configurations.[14-17] Peptides can adopt remarkably different conformations when bound to NPs based upon the number and arrangement of anchoring residues. These changes alter the metal surface exposure for wide variations in catalytic activity. Furthermore, the position of the photoswitch within the peptide could also alter both the photoswitching process and the catalytic performance. In our prior studies, photoswitches were only positioned at the N- or C-terminus of the sequence.[8] Positioning the photoswitch within central region of the peptide may amplify the surface structural differences between the two conformations (*cis* or *trans*). Taken together, numerous biomolecular structural effects are working in concert to control the catalytic capabilities of the materials, presenting great opportunities to fine-tune the reactivity.

Herein we present an in-depth analysis of sequence and structural effects on photo-driven peptide conformational switching and the resultant effects on NP catalytic properties. Through attachment of the azobenzene-based photoswitch into two different peptides at three positions, the N-terminus, C-terminus, or mid-sequence, eight different peptide/NP configurations were examined and compared (Table 1). To probe peptide sequence effects, we selected two well-studied peptides with known affinity for Au: AuBP1 and Pd4 (TSNAVHPTLRHL).[9, 18] In this contribution, the effects of photoswitch attachment at the mid-sequence position in AuBP1 and at all three positions of Pd4 were examined and compared to our previous studies conducted using N- and C-terminus modified AuBP1.[8] Each system was thoroughly characterized for reversible light-driven biointerface reconfiguration by both experimental and computational analyses, which demonstrated that the peptide sequence and the photoswitch position played important roles in controlling the reconfiguration process. Upon confirmation of biointerface reconfiguration capabilities, the catalytic properties of the materials with the photoswitch in the *trans* and *cis* states were assessed using 4-nitrophenol reduction as a model reaction. Interestingly, the reaction rate constants can vary by as much as a factor of four for the same particles in the two different configurations, suggesting that on/off reactivity controlled by light may be possible.

Taken together, these results demonstrate a (bio)organic-inorganic NP system where reactivity can be tuned through optically-activated interfacial conformational changes. These differences are dependent not only upon peptide structure/conformation, but also upon photoswitch placement within the biomolecule. Such results highlight the fine level of control that can result from minor structural differences, which can be readily accessed using materials specific peptides.

Table 1. Peptide sequences denoting position of Cys residue incorporation for MAM coupling

Peptide	Sequence
AuBP1	WAGAKRLVLRRE
CAuBP1	**C**WAGAKRLVLRRE
AuBP1C	WAGAKRLVLRRE**C**
AuBP1[C]	WAGAKR**C**LVLRRE
Pd4	TSNAVHPTLRHL
CPd4	**C**TSNAVHPTLRHL
Pd4C	TSNAVHPTLRHL**C**
Pd4[C]	TSNAVH**C**PTLRHL

Results and Discussion

Peptide-based Materials Fabrication. To probe the effects of peptide sequence and photoswitch incorporation location on biointerfacial reconfiguration and catalytic property manipulation, four new biohybrid molecules were prepared. Initially, to compare with the previously described peptides,[8] the maleimide-azobenzene-maleimide (MAM) unit (Scheme 1) was incorporated at the middle position of the AuBP1 peptide (termed AuBP1[C-MAM]). Additionally, three new species were generated based upon the Pd4 peptide, with the MAM unit at the N-terminus, C-terminus, and middle positions (termed MAM-CPd4, Pd4C-MAM, and Pd4[C-MAM]). To generate each of the MAM-modified peptides, a cysteine residue was incorporated at the 1, 7, or 13 position of the peptide sequence using standard solid-phase synthetic protocols. Upon purification and confirmation of the peptide identity, coupling of the MAM to the peptide was

Scheme 1. Structure of the MAM photoswitch in the (a) *trans* and (b) *cis* conformation.

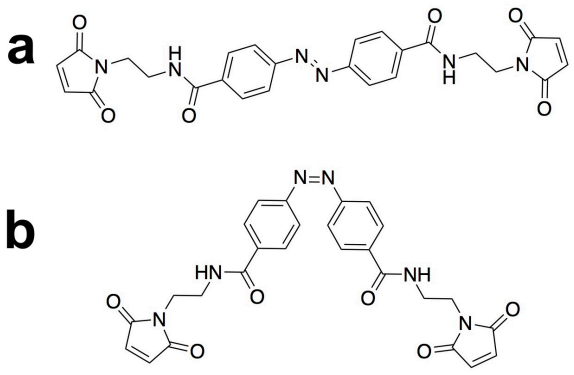

carried out in DMF. A small excess of MAM was present in the reaction to ensure coupling of one photoswitch to one peptide. Once the reaction was complete, the hybrid biomolecules were purified by centrifuge filtration to remove excess reagents and product identity was confirmed by mass spectrometry. Using these newly prepared biomolecules, peptide-capped Au nanoparticles were generated using previously described approaches.[8, 12]

NPs capped with the four new peptides (AuBP1[C-MAM] and all of the Pd4-based systems) were characterized using UV-vis spectroscopy. Previous studies fully analyzed the AuBP1C-MAM- and MAM-CAuBP1-capped materials, which demonstrated nearly identical results.[8] Figure 1a specifically presents the analysis for Au NPs fabricated using the AuBP1[C-MAM]. For the peptide alone (red spectrum), two peaks were observed: one at 320 nm and a second at 450 nm. These two peaks represent the π-π* and n-π* transitions of the azobenzene photoswitch.[11] Upon complexation with the Au^{3+} ions prior to reduction, no substantial change in the spectrum of the materials was observed (blue spectrum); however, reduction with $NaBH_4$ results in a substantial increase in the absorbance of the materials, consistent with Au NP formation (green spectrum). Three key points are notable in this spectrum. First, no plasmon band for the Au NPs was observed suggesting that the nanoparticles were too small to exhibit a well-defined Localized Surface Plasmon Resonance (LSPR) absorbance peak.[19] Second, the n-π* transition of the azobenzene was not evident, as it is masked by the inherent absorbance/scattering of the NPs near 450 nm. Third, the π-π* transition of the hybrid biomolecule remains clearly visible, thus allowing for a readily observable handle to monitor photoswitch isomerization. Nearly identical results were observed with the Pd4-based materials (Figures 1 b-d), where the 320 nm peak was clearly present for each of the peptide-capped materials.

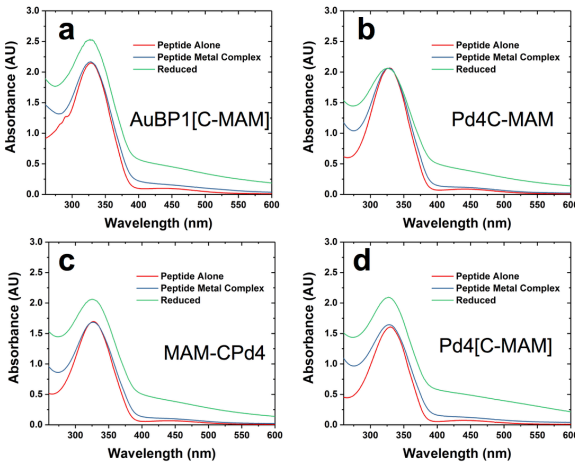

Figure 1: UV-vis absorbance spectra for Au NP production using the (a) AuBP1[C-MAM], (b) Pd4C-MAM, (c) MAMC-Pd4, and (d) Pd4[C-MAM] peptides.

The materials were subsequently imaged by transmission electron microscopy (TEM) to characterize particle size and morphology. When the unmodified parent AuBP1 and Pd4 peptides were previously used to stabilize Au NPs, particle sizes of 4.2 ± 1.1 and 4.3 ± 1.7 nm were prepared.[16, 20] Note that for the AuBP1 peptide, generally spherical particles were prepared; however, for the Pd4-based system, irregularly shaped materials were obtained. TEM images of the Au NPs stabilized with the biohybrid molecules are shown in Figure 2. The materials capped with the AuBP1[C-MAM], Pd4C-MAM, and MAM-CPd4 molecules were generally spherical and small in size with average diameters of 2.8 ± 0.6, 2.5 ± 0.6, and 2.5 ± 0.5 nm, respectively. These values were similar in dimension to the Au NPs capped with the AuBP1C-MAM (2.7±0.7nm) and MAM-CAuBP1 (2.4±0.6 nm) peptides, as shown previously.[8, 12] However, when the MAM unit was positioned at the center of the Pd4 peptide (Pd4[C-MAM]), the AuNPs were notably

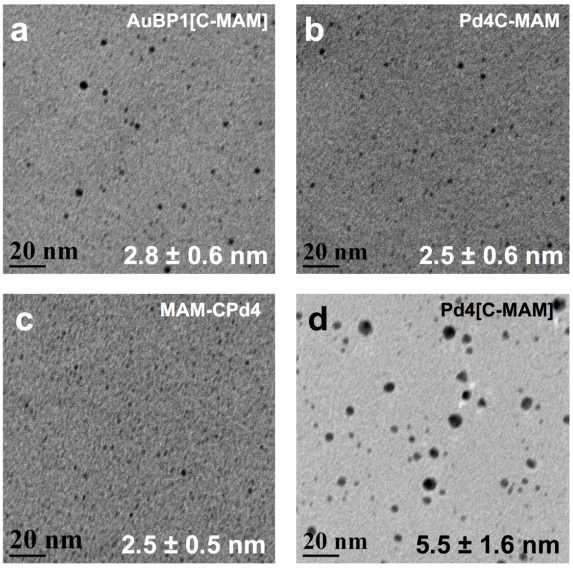

Figure 2. TEM images of the Au NPs passivated using the (a)AuBP1[C-MAM], (b) Pd4C-MAM, I(c) MAM-CPd4, and (d) Pd4[C-MAM] peptides.

larger and more polydisperse in size (5.5 ± 1.6 nm). For each sample, sizing of at least 100 NPs was completed with the MAM held in the *trans* conformation (Supporting Information, Figure S1). Such small sizes are likely the basis of the lack of a significant plasmon band in the UV-vis analysis of the materials.

From the TEM analysis, we note that the Pd4C-MAM- and MAM-CPd4-capped NPs were quite small compared to those capped with the parent Pd4 sequence or the Pd4[C-MAM] biomolecules. This suggests that the position of the MAM within the Pd4 peptide plays a role in controlling the final NP size and structure; however, no clear trends are present

with respect to MAM position and particle size. This behavior is similar to that of the AuBP1 peptide, for which NP sizes differed based upon whether the MAM unit was present in the sequence or not. As such, this presents a clear difference between peptides with and without the MAM, suggesting that the amino acid composition, photoswitch, and MAM position are important for controlling material structure and resultant properties.

After characterizing the NP structure, we examined the ability of the photoswitch to isomerize between the *trans* and *cis* conformations. *Trans*-to-*cis* switching was achieved by UV-illumination, while *cis*-to-*trans* switching employed white light illumination. The azobenzene conformational changes were monitored *via* the 320 nm peak, which diminished in intensity after switching to the *cis* conformation; the 320 nm peak then returns to a higher intensity when the molecule is isomerized back to the *trans* conformation.[11, 21]

Figure 3a presents the photoswitching results for the AuBP1[C-MAM]-capped Au NPs. Prior to the photoswitching process (red spectrum), the materials presented a peak at 320 nm, as anticipated. These particles were then irradiated with UV light for at least 30 min, resulting in the 320 nm peak diminishing in intensity (blue spectrum). The materials were then exposed to white light for 30 min to switch the MAM component back to the *trans* state, which resulted in a restoration of the original absorbance intensity of the 320 nm peak (green spectrum). This trend was demonstrated for all four NP systems, consistent with reversible photoswitching of the azobenzene moiety between the *trans* and *cis* conformations. Note that the photoswitch can be optically switched over multiple cycles without causing particle aggregation, demonstrating persistent NP colloidal stability provided by the hybrid biomolecules.

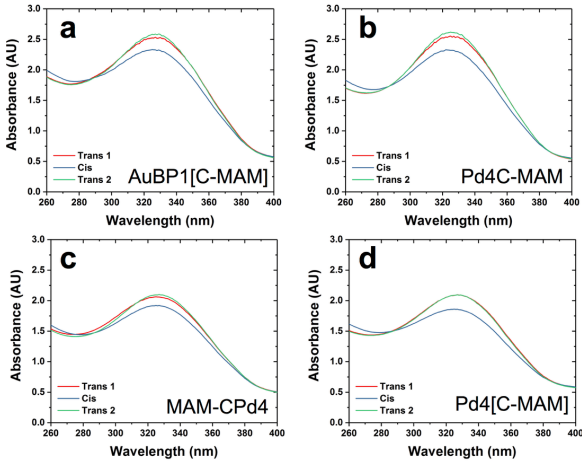

Figure 3. Photoswitching analysis for the Au NPs capped with (a) AuBP1[C-MAM], (b) Pd4C-MAM, (c) MAM-CPd4, and (d)Pd4[C-MAM].

While light is used to intentionally drive photoswitch isomerization, thermal switching of the molecule from the *cis*-to-*trans* conformation can occur. This is based upon the greater stability of the *trans* molecule over the *cis*.[11, 21] As such, the half-life of the four different MAM-modified peptides on the Au NP surface was also monitored using UV-vis absorbance. For this, the NP sample was irradiated with UV light for 30 min to drive *trans* to *cis* conversion. The particles were then kept in the dark at 20 °C and analyzed by UV-vis every 10 min for 16 h to quantify the rate of thermal switching. Consistent with previous studies of the AuBP1C-MAM and MAM-CAuBP1 sequences, long half-lives of 218.8 ± 59.5, 160.7 ± 72.4, 332.6 ± 10.7, and 191.4 ± 42.1 h were determined for the NPs capped with the AuBP1[C-MAM], Pd4C-MAM, MAM-CPd4, and Pd4[C-MAM] peptides, respectively (Supporting Information, Figure S2). Such long half-lives are a result of stabilization of the MAM moiety on the Au surface, which can inhibit the thermally driven conformation change.[8] These results demonstrate that the reactivity observed from the NPs with the biointerface in the *cis* conformation arises from the anticipated configuration and that photoswitch thermal isomerization is not complicating the reactivity analysis.

Molecular Simulation of Peptide Adsorption. Molecular simulations of these molecules adsorbed at the aqueous Au interface showed differences in the degree and modes of surface contact, depending on both the parent peptide sequence and the location of the MAM moiety. In comparison with data from our previous simulations of surface-adsorbed *cis*-AuBP1C-

Table 2. Residue-surface contact data (percentages) for the Pd4/MAM and associated molecules adsorbed on the Au(111) surface, determined from the REST-MD simulations. Colors indicate percentage ranges for ease of comparison.*

Residue	Pd4	Pd4[C]	MAM-CPd4		Pd4C-MAM		Pd4[C-MAM]	
			trans	*cis*	*trans*	*cis*	*trans*	*cis*
C	-	-	63	57	-	-	-	-
T	27	7	22	42	3	9	13	6
S	36	24	27	24	33	24	30	32
N	48	55	27	53	55	60	50	48
A	46	47	23	26	62	48	42	62
V	25	35	34	42	44	13	26	32
HH	78	66	66	73	62	57	77	70
C	-	70	-	-	-	-	72	71
P	28	42	60	28	60	33	70	64
T	33	13	40	20	14	10	20	6
L	31	14	39	54	27	25	19	29
R	44	79	72	60	51	33	39	59
HA	94	91	83	88	79	92	74	84
L	17	13	20	11	22	32	4	8
C	-	-	-	-	79	70	-	-
Mal1			66	79	67	58	65	63
Bnz1			94	34	94	47	93	48
N=N			94	78	94	78	93	71
Bnz2			94	46	94	33	93	26
Mal2			93	90	93	85	88	89

*HA and HH denotes histidine in the unprotonated and protonated states respectively. Further details are provided in the Supporting Information.

MAM and *cis*-MAM-CAuBP1,[12-13, 20] the binding characteristics of *cis*-AuBP1[C-MAM] from our current simulations suggest an overall reduction in surface contact of the MAM unit (Table S1, Supporting Information).[12-13] In contrast, the surface contact of the peptide component of *cis*-AuBP1[C-MAM] was less affected. A similar outcome emerged from comparisons of the three variants in the *trans* state. However, although the MAM unit in *trans*-AuBP1[C-MAM] showed relatively reduced binding, its degree of surface contact was still very high.

Surface adsorption of both the *cis* and *trans* isomers of Pd4C-MAM, MAM-CPd4, and Pd4[C-MAM] was modeled in the present work (summarized in Table 2). We found that the two anchor points identified in earlier work for the parent peptide,[20] namely H6 and H11, broadly featured as surface anchors in all cases. Regardless of its position in the peptide sequence, binding of the MAM unit was similarly strong. When considering all three variants in the *trans* state, the greatest degree of contact for H6 was noted for Pd4[C-MAM]. Comparing this species with the binding data for Pd4[C] (the 13-mer version of the parent Pd4 peptide with a central Cys residue) indicated that the presence of the MAM unit, and not merely the central Cys residue, is responsible for this enhancement. The presence of the central C-MAM unit was also seen to enhance the overall contact of the region containing the H6 and P7 residues. Enhanced contact for this region was maintained for Pd4[C-MAM] in the *cis* conformation as compared to the other two conjugates.

Further trends were noted for Pd4[C-MAM] that were not evident for the other two conjugates. In this regard, the C-terminal portion, LRHL, demonstrated

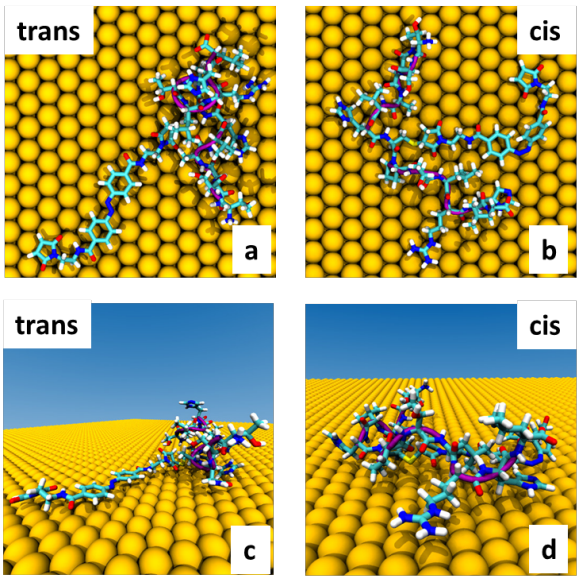

Figure 4. Representative snapshots of Pd4[C-MAM] adsorbed at the aqueous Au(111) interface. Water not shown for clarity. (a) top view of the *trans* isomer, (b) top view of the *cis* isomer, (c) side view of the *trans* isomer, (d) side view of the *cis* isomer.

enhanced contact in the *cis* isomer relative to the *trans* form. This suggests that the *cis* isomer is less disordered when bound to the Au surface as compared to the *trans* form. These findings differ from those for the other two conjugates, MAM-CPd4 and Pd4C-MAM. For these conjugates, no clear trend was noted for the residue-surface contact for the *cis* and *trans* isomers of these species. Representative snapshots of the surface-adsorbed structures of Pd4[C-MAM] in both the *cis* and *trans* form are provided in Figure 4.

In addition to surface contact, we also analyzed the conformational entropic contribution of these surface-adsorbed molecules,[20] which can indicate whether binding is enthalpically- or entropically-driven. As described in the Computational Methods in the Supporting Information, we estimated this by calculating the conformational entropic contribution of the peptide backbone, S_{conf}, summarized in Table 3. A larger value of S_{conf} indicates a greater degree of disorder in the ensemble of adsorbed conformations. For conjugates of both AuBP1 and Pd4, we found that the central location of the MAM unit led to the highest conformational entropic contribution, compared with the N- and C-terminal MAM positions. In all cases except Pd4[C-MAM], the *trans* isomer featured a smaller value of S_{conf} than the corresponding *cis* isomer, reflecting the general trend that strong surface engagement of the MAM unit in the *trans* state restricted the conformational freedom of the peptide backbone. For the Pd4[C-MAM], we noted an unexpected reduction in S_{conf} for the *cis* isomer compared with that of the *trans* state. This finding is consistent with our surface contact analysis presented above.

Table 3. S_{conf} values for the indicated peptide backbone calculated from REST-MD simulations.

	trans	*cis*
AuBP1	2.73	
AuBP1[C]	3.20	
MAM-CAuBP1	2.58	2.89
AuBP1C-MAM	2.52	2.73
AuBP1[C-MAM]	2.90	3.16
Pd4	3.08	
Pd4[C]	3.53	
MAM-CPd4	2.72	2.85
Pd4C-MAM	2.84	3.02
Pd4[C-MAM]	3.23	3.12

Catalytic Activity Modulation *via* Optical Stimulation. Modulation of catalytic reactivity upon reconfiguration of the biointerfaces can arise from differences in exposure of the underlying metallic surface to the reagents in solution. To examine this effect, we employed reduction of 4-nitrophenol (4-NP) to 4-aminophenol (4-AP) as a model reaction. This reaction is

ideal for many reasons, but primarily because it is known to occur directly on the metal surface.[22-23] This feature is critically important for elucidating how changes in the biointerfacial structure drive variations in catalytic activity. Additionally, the reaction is readily monitored using simple UV-vis measurements of reactant consumption. In the presence of excess $NaBH_4$, the Au NPs can catalytically reduce 4-NP to 4-AP, where the reaction progress is followed by the decrease in absorbance intensity of the 4-NP reactant.[23-24]

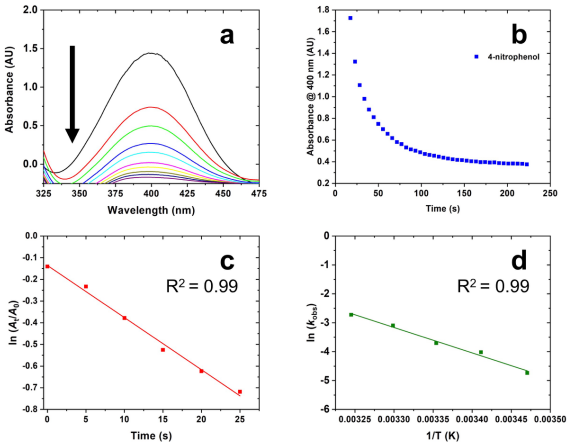

Figure 5. The reduction of 4-NP with Au NPs capped with AuBP1[C-MAM] in the *trans* conformation. Panel (a) presents a collection of UV-vis absorbance spectra over a period of time, showing the characteristic decrease of absorbance near 400 nm related to 4-NP reduction, while panel (b) plots the decrease of absorbance at 400 nm as a function of time. Panel (c) illustrates the determination of the pseudo-first order rate constant *via* a plot of $\ln(A_t/A_0)$ *vs* time. Panel (d) shows the calculation of activation energy *via* an Arrhenius plot.

Figure 5 presents the reaction rate analysis for the AuBP1[C-MAM]-capped Au NPs, while the corresponding Arrhenius analysis for the Au NPs capped with Pd4-based ligands are presented in the Supporting Information, Figure S6. Figure 5a presents UV-vis results demonstrating a decrease in absorbance at 400 nm, the peak associated with the 4-NP reactant. Over time, this peak decreases in intensity, concomitant with an increase in intensity for the peak at 300 nm associated with the 4-AP product. Figure 5b presents the decrease in the 400 nm absorbance as a function of time, while Figure 5c displays a plot of $\ln(A_t/A_0)$ *vs.* time, where A_t represents the absorbance at time t, and A_0 is the initial absorbance. Thus, A_t/A_0 is proportional to the 4-NP concentration. The analysis illustrated in Figure 5 has been previously employed by many research groups.[22, 25-26] Linear fitting of the plot in Figure 5c provides a pseudo first order rate constant (k_{obs}). This approach was completed for catalytic reactions over a temperature range of 15 – 35 °C. The resulting temperature-dependent k_{obs} values were then used in the Arrhenius plots like that

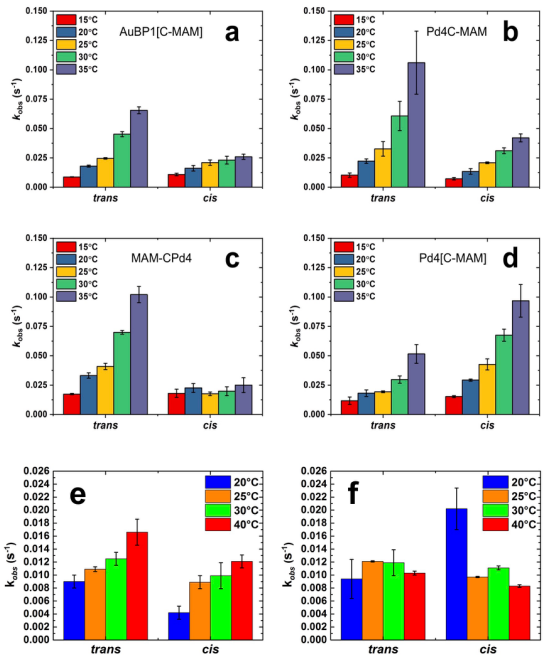

Figure 6. k_{obs} values for the reduction of 4-NP catalyzed by Au NPs capped with (a) AuBP1[C-MAM], (b) Pd4C-MAM, (c) MAMC-Pd4 , and (d) Pd4[C-MAM]. Parts (e and f) present the catalytic data previously published from reference 8 for Au NPs capped with (e) AuBP1C-MAM and (f) MAM-AuBP1. This data is shown for ease of comparison.

shown in of Figure 5d to determine activation energies (E_a) and pre-exponential factors (A).

Using the process shown in Figure 5, the *pseudo* first order rate constants of for Au NPs stabilized by AuBP1[C-MAM] were calculated at the selected reaction temperatures and are presented in Figure 6a and Table S2 of the Supporting Information. When the azobenzene molecule in the peptide was in the *trans* configuration, the k_{obs} values ranged from $(8.8 \pm 0.2) \times 10^{-3}$ s^{-1} to $(65.6 \pm 2.9) \times 10^{-3}$ s^{-1} over the selected temperature range; however, when the same Au NPs were used to drive the reaction with the MAM in the *cis* state, the rate constants ranged from $(10.9 \pm 1.0) \times 10^{-3}$ s^{-1} to $(25.9 \pm 2.2) \times 10^{-3}$ s^{-1}. Activation energies calculated from this data were 73.2 ± 5.2 kJ/mol and 30.9 ± 7.2 kJ/mol for the *trans* and *cis* conformations, respectively.

In previous experiments, Au NPs were prepared with AuBP1 peptide that positioned the photoswitch at the N- or C-terminus, denoted as MAM-CAuBP1 and AuBP1C-MAM.[8] From those catalytic trials (Figures 6 e and f), the reduction of 4-NP was monitored across a temperature range of 20 to 40 °C, and measured at four temperatures. Particles passivated with AuBP1C-MAM (Figure 6e) while in the *trans* conformation had k_{obs} ranging from $(9.0 \pm 1.3) \times 10^{-3}$ to $(16.6 \pm 0.7) \times 10^{-3}$ s^{-1}. When the photoswitch was isomerized to the *cis* conformation, a significantly smaller range of rate constants was observed, ranging from (4.2 ±

0.7) × 10^{-3} s^{-1} to (12.1 ± 1.1) × 10^{-3} s^{-1}. From this data, the calculated activation energies were 23.0 ± 3.5 and 35.3 ± 4.0 kJ/mol, for the *trans* and *cis* conformations, respectively. When the photoswitch was placed at the C-terminus of the AuBP1 peptide, neither photoswitch conformation allowed for determination of an activation energy (Figure 6f); however, when MAM-CAuBP1 was in the *trans* conformation, the k_{obs} values appeared to be relatively steady across the specified temperature range, with an average value of (10.9 ± 1.3) × 10^{-3} s^{-1}.

Pseudo first order rate constants for the Au NPs capped with Pd4C-MAM ligands were determined in a similar manner and are presented in Figure 6b. For this system in the *trans* conformation, the k_{obs} values ranged from (10.9 ± 1.0) × 10^{-3} s^{-1} to (106.1 ± 26.8) × 10^{-3} s^{-1}, while in the *cis* conformation, the k_{obs} values spanned a significantly smaller range of (7.2 ± 1.1) × 10^{-3} s^{-1} to (42.1 ± 3.3) × 10^{-3} s^{-1}. These values show a 2.5-fold difference in the rate constants at 35 °C. From this analysis, activation energies of 83.7 ± 6.9 kJ/mol and 64.6 ± 4.4 kJ/mol were determined for *trans* and *cis* conformations respectively. *Pseudo* first order rate constants were also extracted for the Au NPs capped with MAM-CPd4 peptide (Figure 6c). For this system in the *trans* configuration, the rate varied from (17.4 ± 0.5) × 10^{-3} s^{-1} at 15 °C to (102.0 ± 6.8) × 10^{-3} s^{-1} at 35 °C. Interestingly, for the MAM-CPd4-capped Au NPs in the *cis* conformation, the k_{obs} values did not change with temperature; an average pseudo first order rate constant of ~20.6×10^{-3} s^{-1} was determined, regardless of the reaction temperature. This suggests that a potentially unique surface structure on these materials with the peptide in the *cis* form may be occurring. That said, a roughly four-fold enhancement in reactivity was noted for these materials with the peptides in the *trans* conformation over the *cis* at 35 °C. While an activation energy cannot be calculated for the NPs in the *cis* configuration, the E_a value for the *trans*-based NPs was 63.3 ± 2.9 kJ/mol.

For the Au NPs passivated with Pd4[C-MAM], a notably different reaction trend was observed (Figure 6d). For this system, Au NPs with the peptide overlayer in the *cis* conformation displayed enhanced reactivity as compared to the NPs with the peptide in the *trans* configuration. More specifically, the reaction rates for the *cis* Pd4[C-MAM] system ranged from (15.3 ± 1.0) × 10^{-3} s^{-1} at 15 °C to (96.8 ± 13.9) × 10^{-3} s^{-1} at 35 °C. This resulted in an activation energy of 66.9 ± 4.2 kJ/mol. For the Au NPs in the *trans* conformation, the reaction rates increased from (11.8 ± 3.2) × 10^{-3} s^{-1} to (51.6 ± 7.9) × 10^{-3} s^{-1} over the same temperature range, resulting in an E_a value of 50.8 ± 1.9 kJ/mol.

The above results show that, not only are reaction rates different for the same NPs with the peptide in the *cis* and *trans* states, but the temperature dependence of reaction rates differs dramatically between *cis* and *trans* states. In general, the isomerization state producing the higher reaction rates also exhibited higher activation energy. This is somewhat unexpected, as it implies a higher energetic barrier to reaction for the state with a higher reaction rate. Generally, catalysts work by lowering activation barriers to facilitate the reaction, and thus lower activation barriers are characteristic of high reaction rates. However, the activation energy alone does not determine the reaction rate. The frequency factor (A) was determined from the y-intercept of the Arrhenius plot (Figure 5d) for each catalytic system. A is related to the frequency with which the reactant approaches the activation barrier. Note that A does not discriminate between successful and non-successful approaches, rather, it reflects the total number of approaches. The frequency factor is also related to the entropy difference between the reactants and transition state structure. A large value of A implies relatively high entropy of the reacting system near the barrier to reaction, or a relatively high density of states or pathways leading to reaction.

For the AuBP1[C-MAM]-capped Au NPs, a large A value of 1.60 × 10^{8} s^{-1} was determined with the peptide in the *trans* state; however, the same NPs with the ligands in the *cis* conformation yielded a significantly smaller frequency factor of 5.04 × 10^{3} s^{-1}. This represents a difference of five orders of magnitude and reflects a one hundred thousand-fold higher rate of reaction "attempts" in the *trans* state. Such effects are not too surprising as changes in the biomolecular overlayer structure are being exploited to change the reactivity. As such, access to the catalytic surface is anticipated to change, giving rise to the substantial differences in the A values, which directly correlates to the differences in reactivity.

Similar trends were noted for the Pd4C-MAM- and Pd4[C-MAM]-capped Au NPs. Note that a correlation could not be achieved for the MAM-CPd4-capped materials due to their unique reactivity. When considering the Pd4C-MAM-based NPs specifically, notably different frequency factors were calculated: 1.64 × 10^{13} and 4.12 × 10^{9} s^{-1} for the NPs with the peptide in the *trans* and *cis* structure, respectively. Again, the higher A value for the *trans* conformation was the source of higher k_{obs} values. For the Pd4[C-MAM]-capped Au NPs, the situation was reversed. The materials with the *cis* form of the peptide were the most active. When the A values were calculated for this system, the optimal *cis*-based materials presented the higher frequency factor (2.28 × 10^{10} s^{-1}) by approximately three orders of magnitude over the value for the *trans*-based structures (1.82 × 10^{7} s^{-1}).

When considering the MAM-CPd4-capped Au NPs, a unique situation is observed. While a typical Arrhenius-type increase in the k_{obs} values with increasing temperature was noted for the particles with the peptide in the *trans* conformation, the rate constants for the same NPs with the peptide in the *cis* conformation displayed nearly constant reactivity over the studied

temperature range. For this system, the materials remain stable and dispersed in solution throughout the duration of the reaction, without any noticeable changes, indicating that the particle structures remained intact. Such stability is also supported by the recyclability studies discussed below. This reactivity difference suggests that the MAM-CPd4-capped NPs present a surface structure that inhibits the reactivity when present in the *cis* conformation, and that this structure is independent of temperature over the range considered here. As such, the four-fold differences in k_{obs} values at 35 °C likely arise from substantial biointerfacial structural differences.

Across the majority of the different NP systems, over the temperature range employed in this study, higher rate constants arose from the conformation with the higher frequency factor and higher activation energy. Differences in the catalytic activity between the isomerization states are attributed to the peptide/NP interface that changes structure based upon the conformation of the MAM unit. In each case, one conformation dramatically increases the frequency of reaction attempts, providing many more pathways for the reaction to occur, but also a higher barrier to reaction. The simplest explanation for this would be that in each case, one isomer provides much greater access to the underlying metal surface. Such effects were clearly evident for three of the NP systems; however, notable differences were observed for the MAM-CPd4-capped NPs which displayed a biointerface structure in the *cis* conformation that strongly inhibited reagent metal surface access at all temperatures. The large differences in both activation energy and frequency factor imply substantially different reaction paths for the two isomerization states.

The recyclability of the NPs was also evaluated by employing the materials in six consecutive reduction reactions at 25 °C (Figure 7). In general, the reactivity of the materials was stable over the selected number of catalytic cycles. Interestingly, a jump in reactivity after the first catalytic cycle was noted for each system. Such changes have been observed previously and may arise from restructuring of the metal atoms on the NP surface in response to the first reaction.[23] Nevertheless, the NPs remain highly reactive and recyclable for at least six cycles, regardless of the peptide surface conformation.

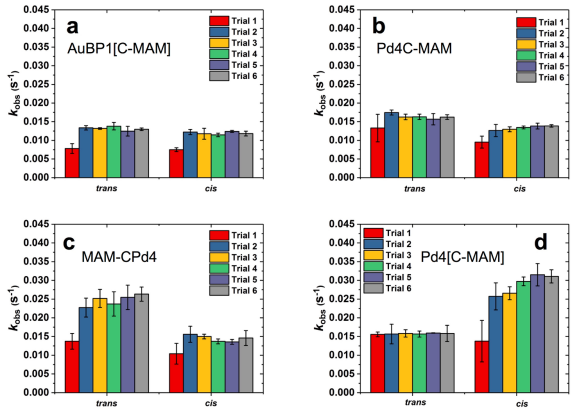

Figure 7: Recyclability studies of for multiple 4-NP reduction reactions driven via Au NPs capped with (a) AuBP1[C-MAM], (b) Pd4C-MAM, (c) MAM-CPd4, and(d) Pd4[C-MAM].

The observed changes in reactivity are controlled by the structure of the peptide overlayer on the NP surface, which is substantially affected by the peptide sequence and the position of the photoswitch. Clear differences in reactivity are observed when comparing the NPs capped with either the AuBP1- or Pd4-based hybrid biomolecules possessing the MAM unit at the same position, as anticipated. Interestingly, when comparing the materials capped with the Pd4-derived biomolecules, a unique reactivity trend can be observed based upon the MAM position. When the photoswitch is included at the N-terminus (MAM-CPd4), reactivity for NPs with the bio-overlayer in the *trans* conformation is greater than the same materials in the *cis*. When the MAM is positioned in the central position, as in the Pd4[C-MAM] sequence, an opposite trend is observed where greater reactivity for the NPs in the *cis* conformation is observed as compared to the *trans*. Finally, for the Pd4C-MAM NPs that integrate the azobenzene moiety at the C-terminus, an unusual trend in reactivity is observed. In this case, the NPs in the *trans* conformation display great reduction capabilities; however, when the bio-overlayer is photoswitched to the *cis* conformation, the reactivity is nearly inhibited at all reaction temperatures. This demonstrates how the position of the photoswitch can be employed to directly modulate the catalytic reactivity as a function of the isomerization state. We note, however, that this trend is specific for the Pd4 sequence, and different trends are likely to occur for different peptides.

Our combined experimental and modeling data clearly show that the placement of the azobenzene MAM unit within the peptide affects the trends in structural changes as a function of MAM isomerization state. This is reflected in the catalytic activity data, where larger reaction rate constants were observed for the Pd4C-MAM- and MAM-CPd4-capped Au nanoparticles for the *trans* conformation relative to the *cis* state. The opposite was observed for the Pd4[C-MAM] system that displayed greater reactivity for the *cis* conformation relative to *trans*. Such differences were consistent with the modeling data that indicated that the MAM-CPd4 featured an unexpected increase in peptide conformational order in the *cis* structure, potentially giving rise to a ligand layer structure that blocked the surface. The opposite trend was observed for the other two conjugates of Pd4, where conformational disorder increased for the *cis* isomer compared with *trans*.

Conclusion

In summary, our combined experimental and computational analyses demonstrate that positioning of non-natural functional moieties into peptides can directly modulate the emergent material properties at the biotic/abiotic interface. In this specific instance we showed that the catalytic capabilities were altered through site-selective integration of the azobenzene photoswitch and the photoswitch isomerization state. This allowed for substantial modulation of the catalytic properties of peptide-capped Au NPs, where up to a four-fold difference in reactivity can be accessed as a function of the light-driven switching of the peptide conformation. Additionally, we have demonstrated a system (MAM-CPd4) that presents a pathway toward potential on/off reactivity where the biomolecule overlayer in one conformation greatly inhibits the overall reactivity in a temperature-independent manner. Such results could prove to be important for both catalyst design and activation, as well as in the development of new functional biomolecules for the production of nanomaterials with applications in sensing, energy, and therapeutics.

Materials and Methods

Materials. $HAuCl_4$ was purchased from Acros Organics, and $NaBH_4$ was obtained from Sigma-Aldrich. Trifluoroacetic acid (TFA), 4-nitrophenol (4-NP), and tri-isopropyl silane (TIS) were sourced from Alfa Aesar, while methanol, acetonitrile, and *N,N*-dimethylformamide (DMF) were acquired from BDH. Lastly, piperidine, *N,N*-diisopropylethylamine (DIPEA), *N,N,N',N'*-tetramethyl-O-(1H-benzotriazol-1-yl)uronium hexafluorophosphate HBTU, hydroxybenzotriazole (HOBt), Wang resins, and FMOC-protected amino acids were purchased from Advanced Chemtech. All experiments were conducted using Ultrapure water (18.2 MΩ•cm) and all reagents were used as supplied.

Peptide Synthesis and Azobenzene Coupling: Standard solid phase FMOC protocols were used to synthesize all peptides using a TETRAS peptide synthesizer (Creosalus).[27] Peptide cleavage from the resin was achieved using TFA/EDT/thioanisole/anisole (90:3:5:2) for 4 h, followed by purification *via* reverse-phase HPLC (Waters Co. Delta 600 with 2498 Detector). Once purified, the identities of all peptides were confirmed through ESI mass spectrometry.

The maleimide-azobenzene-maleimide (MAM) molecule was synthesized and purified using previously published protocols.[12] Coupling of the photoswitch to the peptide was achieved *via* standard thiol-maleimide coupling protocols, with an excess of MAM present to encourage single peptide to MAM pairings.[12] After coupling, the reaction mixture was purified using centrifuge filtration (Amicon Ultra-0.5 Centrifugal Filter Devices 3000 NMWL (Millipore)). The retentate was diluted with ~2 mL of water and then lyophilized.

Peptide-Capped Au NP Synthesis. Standard synthesis protocols were employed to generate the peptide-capped Au NPs.[8, 12] Briefly, 10 μL of $HAuCl_4$ (0.1 M) was diluted with 2.96 mL of water, followed by addition of 2 mL of the peptide-MAM conjugate in water (stock solution is 0.25 mM). The mixture was stirred on the bench top for 15 min to allow for the metal ions to complex with the peptide. Next, 30 μL of freshly prepared $NaBH_4$ (0.10 mM) was added to the mixture and swirled by hand three times. The reaction was then allowed to sit undisturbed for 1 h on the benchtop.

Characterization. Once prepared, the NPs were allowed to sit for 24 h prior to optical analysis. Each sample was analyzed using an Agilent 8453 UV-vis spectrophotometer with 1 cm path length quartz cuvettes. TEM imaging was conducted using a JEOL JEM-2010 TEM at a 200kV working voltage. All of the TEM samples were prepared by drop casting 10 μL of the NP solution onto a carbon coated copper TEM grid. Image analysis was conducted to determine NP sizes using the ImageJ software. At least 100 NPs per sample were counted over multiple regions on the TEM grid.

Catalytic Reaction Analysis. The synthesized NPs were tested for their catalytic activity *via* the reduction of 4-NP using previously reported methods.[8] Briefly, in a 1 cm path length quartz cuvette, 975 μL of water was mixed with 450 μL of the NP solution, yielding a 60 μM NP solution based upon total metal concentration. To this solution 25 μL of freshly prepared $NaBH_4$ was added, resulting in a 60 mM concentration. The solution was allowed to sit for 10 min before 50 μL of 4-NP (3.6 mM) was mixed into the solution. In this reaction, a concentration of 120 μM of the 4-NP reagent was present, thus the $NaBH_4$ was in substantial excess. After all additions, the final volume of the reaction mixture was 1.5 mL. For the reaction analysis, UV-vis spectra were recorded at 400 nm every 5 s to monitor reaction progress.

Molecular Simulations. The surface-adsorbed conformational ensembles of all Pd4- and AuBP1-based hybrid molecules were predicted using Replica Exchange with Solute Tempering (REST)[28-29] molecular dynamics (MD) simulations. We performed a REST-MD simulation for each of the hybrid molecules AuBP1[C], AuBP1[C-MAM], Pd4[C], MAM-CPd4, Pd4C-MAM, and Pd4[C-MAM] adsorbed at the aqueous planar Au (111) interface. Each REST-MD simulation comprised a single hybrid molecule adsorbed at the Au (111) interface in the presence of liquid water. Earlier studies indicated that the Au(111) surface is a reasonable surrogate for the polycrystalline Au substrate, as used in the QCM experiments.[30-32] The polarizable GolP-CHARMM force-field,[33-34] the CHARMM22* force-field,[35-36] and the modified TIP3P potential[37-38] were used to describe the interactions involving the Au surface, the hybrid molecule, and water, respectively. The GolP-CHARMM force-field has been recently demonstrated to give results consistent with the experimentally-determined binding free energy of the AuBP1 peptide at the aqueous Au interface.[30] We used the Gromacs[39] software package for all of the simulations described herein. Additional details, including simulation analyses, and evidence of REST-MD sampling efficacy and sampling equilibration, can be found in the 'Computational Methodology' section of the Supporting Information.

ASSOCIATED CONTENT

Supporting Information

Particle size distribution histograms, additional catalytic analyses, residue-surface contact data predicted for the AuBP1-based hybrid molecules, and Computational Methodology.

AUTHOR INFORMATION

Corresponding Author

MRK – knecht@miami.edu

Present Addresses

†ZEH: School of Chemistry and Biosciences, University of Bradford, Bradford, BD7 1DP, U.K.

Author Contributions

The manuscript was written through contributions of all authors. All authors have given approval to the final version of the manuscript.

Funding Sources

This material is based upon work supported by the Air Office of Scientific Research, grant number FA9550-12-1-0226.

ACKNOWLEDGMENT

TRW gratefully acknowledges computing resources from the National Computational Infrastructure (NCI), which is supported by the Australian Government.

REFERENCES

1. Friend, C. M.; Xu, B. Heterogeneous Catalysis: A Central Science for a Sustainable Future. *Acc. Chem. Res.* **2017,** *50*, 517-521.

2. Campelo Juan , M.; Luna, D.; Luque, R.; Marinas José , M.; Romero Antonio , A. Sustainable Preparation of Supported Metal Nanoparticles and Their Applications in Catalysis. *ChemSusChem* **2009,** *2*, 18-45.

3. Sankar, M.; Dimitratos, N.; Miedziak, P. J.; Wells, P. P.; Kiely, C. J.; Hutchings, G. J. Designing Bimetallic Catalysts for a Green and Sustainable Future. *Chem. Soc. Rev.* **2012,** *41*, 8099-8139.

4. Walsh, T. R.; Knecht, M. R. Biointerface Structural Effects on the Properties and Applications of Bioinspired Peptide-Based Nanomaterials. *Chem. Rev.* **2017,** *117*, 12641-12704.

5. Chi, Q.; Ford, M. J.; Halder, A.; Hush, N. S.; Reimers, J. R.; Ulstrup, J. Sulfur Ligand Mediated Electrochemistry of Gold Surfaces and Nanoparticles: What, How, and Why. *Curr. Opin. Electrochem.* **2017,** *1*, 7-15.

6. Johnston, B. D.; Kreyling, W. G.; Pfeiffer, C.; Schäffler, M.; Sarioglu, H.; Ristig, S.; Hirn, S.; Haberl, N.; Thalhammer, S.; Hauck, S. M.; Semmler-Behnke, M.; Epple, M.; Hühn, J.; Pino, P. D.; Parak, W. J. Colloidal Stability and Surface Chemistry Are Key Factors for the Composition of the Protein Corona of Inorganic Gold Nanoparticles. *Adv. Funct. Mater.* **2017,** *27*, 1701956.

7. Suchomel, P.; Kvitek, L.; Prucek, R.; Panacek, A.; Halder, A.; Vajda, S.; Zboril, R. Simple Size-Controlled Synthesis of Au Nanoparticles and Their Size-Dependent Catalytic Activity. *Sci. Rep.* **2018,** *8*, 4589.

8. Lawrence, R. L.; Scola, B.; Li, Y.; Lim, C.-K.; Liu, Y.; Prasad, P. N.; Swihart, M. T.; Knecht, M. R. Remote Optically Controlled Modulation of Catalytic Properties of Nanoparticles through Reconfiguration of the Inorganic/Organic Interface. *ACS Nano* **2016,** *10*, 9470-9477.

9. Hnilova, M.; Oren, E. E.; Seker, U. O. S.; Wilson, B. R.; Collino, S.; Evans, J. S.; Tamerler, C.; Sarikaya, M. Effect of Molecular Conformations on the Adsorption Behavior of Gold-Binding Peptides. *Langmuir* **2008,** *24*, 12440-12445.

10. Palafox-Hernandez, J. P.; Tang, Z.; Hughes, Z. E.; Li, Y.; Swihart, M. T.; Prasad, P. N.; Walsh, T. R.; Knecht, M. R. Comparative Study of Materials-Binding Peptide Interactions with Gold and Silver Surfaces and Nanostructures: A Thermodynamic Basis for Biological Selectivity of Inorganic Materials. *Chem. Mater.* **2014,** *26*, 4960-4969.

11. Bandara, H. M. D.; Burdette, S. C. Photoisomerization in Different Classes of Azobenzene. *Chem. Soc. Rev.* **2012,** *41*, 1809-1825.

12. Tang, Z.; Lim, C.-K.; Palafox-Hernandez, J. P.; Drew, K. L. M.; Li, Y.; Swihart, M. T.; Prasad, P. N.; Walsh, T. R.; Knecht, M. R. Triggering Nanoparticle Surface Ligand Rearrangement Via External Stimuli: Light-Based Actuation of Biointerfaces. *Nanoscale* **2015,** *7*, 13638-13645.

13. Palafox-Hernandez, J. P.; Lim, C.-K.; Tang, Z.; Drew, K. L. M.; Hughes, Z. E.; Li, Y.; Swihart, M. T.; Prasad, P. N.; Knecht, M. R.; Walsh, T. R. Optical Actuation of Inorganic/Organic Interfaces: Comparing Peptide-Azobenzene Ligand Reconfiguration on Gold and Silver Nanoparticles. *ACS Appl. Mater. Interfaces* **2016,** *8*, 1050-1060.

14. Bedford, N. M.; Hughes, Z. E.; Tang, Z.; Li, Y.; Briggs, B. D.; Ren, Y.; Swihart, M. T.; Petkov, V. G.; Naik, R. R.; Knecht, M. R.; Walsh, T. R. Sequence-Dependent Structure/Function Relationships of Catalytic Peptide-Enabled Gold Nanoparticles Generated under Ambient Synthetic Conditions. *J. Am. Chem. Soc.* **2016,** *138*, 540-548.

15. Spicer, C. D.; Jumeaux, C.; Gupta, B.; Stevens, M. M. Peptide and Protein Nanoparticle Conjugates: Versatile Platforms for Biomedical Applications. *Chem. Soc. Rev.* **2018,** *47*, 3574-3620.

16. Coppage, R.; Slocik, J. M.; Briggs, B. D.; Frenkel, A. I.; Naik, R. R.; Knecht, M. R. Determining Peptide Sequence Effects That Control the Size, Structure, and Function of Nanoparticles. *ACS Nano* **2012,** *6*, 1625-1636.

17. Lévy, R.; Thanh, N. T. K.; Doty, R. C.; Hussain, I.; Nichols, R. J.; Schiffrin, D. J.; Brust, M.; Fernig, D. G. Rational and Combinatorial Design of Peptide Capping Ligands for Gold Nanoparticles. *J. Am. Chem. Soc.* **2004,** *126*, 10076-10084.

18. Pandey, R. B.; Heinz, H.; Feng, J.; Farmer, B. L.; Slocik, J. M.; Drummy, L. F.; Naik, R. R. Adsorption of Peptides (A3, Flg, Pd2, Pd4) on Gold and Palladium Surfaces by a Coarse-Grained Monte Carlo Simulation. *Phys. Chem. Chem. Phys.* **2009,** *11*, 1989-2001.

19. Kim, Y.-G.; Oh, S.-K.; Crooks, R. M. Preparation and Characterization of 1−2 Nm Dendrimer-Encapsulated Gold Nanoparticles Having Very Narrow Size Distributions. *Chem. Mater.* **2004,** *16*, 167-172.

20. Tang, Z.; Palafox-Hernandez, J. P.; Law, W.-C.; Hughes, Z. E.; Swihart, M. T.; Prasad, P. N.; Knecht, M. R.; Walsh, T. R. Biomolecular Recognition Principles for Bionanocombinatorics: An Integrated Approach to Elucidate Enthalpic and Entropic Factors. *ACS Nano* **2013,** *7*, 9632-9646.

21. Beharry, A. A.; Woolley, G. A. Azobenzene Photoswitches for Biomolecules. *Chem. Soc. Rev.* **2011,** *40*, 4422-4437.

22. Wunder, S.; Polzer, F.; Lu, Y.; Mei, Y.; Ballauff, M. Kinetic Analysis of Catalytic Reduction of 4-Nitrophenol by Metallic Nanoparticles Immobilized in Spherical Polyelectrolyte Brushes. *J. Phys. Chem. C* **2010,** *114*, 8814-8820.

23. Wunder, S.; Lu, Y.; Albrecht, M.; Ballauff, M. Catalytic Activity of Faceted Gold Nanoparticles Studied by a Model Reaction: Evidence for Substrate-Induced Surface Restructuring. *ACS Catal.* **2011,** *1*, 908-916.

24. Gu, S.; Wunder, S.; Lu, Y.; Ballauff, M.; Fenger, R.; Rademann, K.; Jaquet, B.; Zaccone, A. Kinetic Analysis of the Catalytic Reduction of 4-Nitrophenol by Metallic Nanoparticles. *J. Phys. Chem. C* **2014,** *118*, 18618-18625.

25. Zhao, P.; Feng, X.; Huang, D.; Yang, G.; Astruc, D. Basic Concepts and Recent Advances in Nitrophenol Reduction by Gold- and Other Transition Metal Nanoparticles. *Coord. Chem. Rev.* **2015,** *287*, 114-136.

26. Dai, Y.; Yu, P.; Zhang, X.; Zhuo, R. Gold Nanoparticles Stabilized by Amphiphilic Hyperbranched Polymers for Catalytic Reduction of 4-Nitrophenol. *J. Catal.* **2016,** *337*, 65-71.

27. C. Chan, W.; White, P. D., *Fmoc Solid-Phase Peptide Synthesis: A Practical Approach*; 2000.

28. Terakawa, T.; Kameda, T.; Takada, S. On Easy Implementation of a Variant of the Replica Exchange with Solute Tempering in Gromacs. *J. Comput. Chem.* **2010,** *32*, 1228-1234.

29. Wright, L. B.; Walsh, T. R. Efficient Conformational Sampling of Peptides Adsorbed onto Inorganic Surfaces: Insights from a Quartz Binding Peptide. *Phys. Chem. Chem. Phys.* **2013,** *15*, 4715-4726.

30. Wright, L. B.; Palafox-Hernandez, J. P.; Rodger, P. M.; Corni, S.; Walsh, T. R. Facet Selectivity in Gold Binding Peptides: Exploiting Interfacial Water Structure. *Chem. Sci.* **2015,** *6*, 5204-5214.

31. Hughes, Z. E.; Nguyen, M. A.; Li, Y.; Swihart, M. T.; Walsh, T. R.; Knecht, M. R. Elucidating the Influence of Materials-Binding Peptide Sequence on Au Surface Interactions and Colloidal Stability of Au Nanoparticles. *Nanoscale* **2017,** *9*, 421-432.

32. Hughes, Z. E.; Kochandra, R.; Walsh, T. R. Facet-Specific Adsorption of Tripeptides at Aqueous Au Interfaces: Open Questions in Reconciling Experiment and Simulation. *Langmuir* **2017,** *33*, 3742-3754.

33. Wright, L. B.; Rodger, P. M.; Corni, S.; Walsh, T. R. Golp-Charmm: First-Principles Based Force Fields for the Interaction of Proteins with Au(111) and Au(100). *J. Chem. Theory Comput.* **2013,** *9*, 1616-1630.

34. Wright, L. B.; Rodger, P. M.; Walsh, T. R.; Corni, S. First-Principles-Based Force Field for the Interaction of Proteins with Au(100)(5 × 1): An Extension of Golp-Charmm. *J. Phys. Chem. C* **2013,** *117*, 24292-24306.

35. MacKerell, A. D.; Bashford, D.; Bellott, M.; Dunbrack, R. L.; Evanseck, J. D.; Field, M. J.; Fischer, S.; Gao, J.; Guo, H.; Ha, S.; Joseph-McCarthy, D.; Kuchnir, L.; Kuczera, K.; Lau, F. T. K.; Mattos, C.; Michnick, S.; Ngo, T.; Nguyen, D. T.; Prodhom, B.; Reiher, W. E.; Roux, B.; Schlenkrich, M.; Smith, J. C.; Stote, R.; Straub, J.; Watanabe, M.; Wiórkiewicz-Kuczera, J.; Yin, D.; Karplus, M. All-Atom Empirical Potential for Molecular Modeling and Dynamics Studies of Proteins. *J. Phys. Chem. B* **1998,** *102*, 3586-3616.

36. Piana, S.; Lindorff-Larsen, K.; Shaw, David E. How Robust Are Protein Folding Simulations with Respect to Force Field Parameterization? *Biophys. J.* **2011,** *100*, L47-L49.

37. Jorgensen, W. L.; Chandrasekhar, J.; Madura, J. D.; Impey, R. W.; Klein, M. L. Comparison of Simple Potential Functions for Simulating Liquid Water. *J. Chem. Phys.* **1983,** *79*, 926-935.

38. Neria, E.; Fischer, S.; Karplus, M. Simulation of Activation Free Energies in Molecular Systems. *J. Chem. Phys.* **1996,** *105*, 1902-1921.

39. Wennberg, C. L.; Murtola, T.; Páll, S.; Abraham, M. J.; Hess, B.; Lindahl, E. Direct-Space Corrections Enable Fast and Accurate Lorentz–Berthelot Combination Rule Lennard-Jones Lattice Summation. *J. Chem. Theory Comput.* **2015,** *11*, 5737-5746.

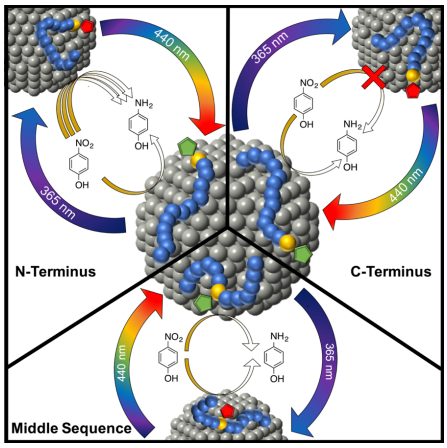
440 nm
365 nm
NO2
NH2
OH
365 nm
440 nm
N-Terminus
C-Terminus
440 nm
365 nm
Middle Sequence